Journal of Catalysis 279 (2011) 111–122

Contents lists available at ScienceDirect

Journal of Catalysis

journal homepage: www.elsevier.com/locate/jcat

Modification of Fe–SiO_2 interaction with zirconia for iron-based Fischer–Tropsch catalysts

Ming Qing [a,b,c], Yong Yang [a,b,*], Baoshan Wu [a,b], Jian Xu [b], Chenghua Zhang [a,b], Peng Gao [b], Yongwang Li [a,b]

[a] State Key Laboratory of Coal Conversion, Institute of Coal Chemistry, Chinese Academy of Sciences, Taiyuan 030001, People's Republic of China
[b] National Engineering Laboratory for Indirect Coal Liquefaction, Institute of Coal Chemistry, Chinese Academy of Sciences, Taiyuan 030001, People's Republic of China
[c] Graduate School of the Chinese Academy of Sciences, Beijing 100039, People's Republic of China

ARTICLE INFO

Article history:
Received 7 October 2010
Revised 17 December 2010
Accepted 8 January 2011
Available online 12 February 2011

Keywords:
Fischer–Tropsch synthesis
Fe–SiO_2 interaction
Zirconia modification
Fourier transform infrared spectroscopy

ABSTRACT

The modification of Fe–SiO_2 interaction in iron catalysts for Fischer–Tropsch synthesis (FTS) by the incorporation of ZrO_2 was investigated by Fourier transform infrared spectroscopy, X-ray photoelectron spectroscopy, temperature-programmed reduction, powder X-ray diffraction, transmission electronic microscopy, and Mössbauer spectroscopy. The results indicated that the strong Fe–SiO_2 interaction could be explained in terms of the formation of Fe–O–Si bonds between iron and SiO_2, and these bonds were effectively weakened by ZrO_2, which consequently enhanced the reduction and carburization of the catalyst and improved the stability of the iron carbides formed. FTS performances, tested in a fixed-bed reactor, showed that both the activity and the C_5^+ selectivity of the Zr-modified catalysts first increased, passed a maximum at Zr loading of 100Fe/20SiO_2–20ZrO_2 with increasing zirconia, and then decreased dramatically at higher Zr loadings. The acid content in the water phase decreased, while the alcohol content increased with the addition of zirconia.

1. Introduction

Silica is one of the most commonly employed supports or binders in iron-based Fischer–Tropsch synthesis (FTS) catalyst [1–3]. The incorporation of SiO_2 into iron catalysts helps to hinder the iron particles' growth from agglomeration or sintering during thermal treatment and reaction [2,3] and to increase the attrition resistance of the samples [4]. Moreover, the strong Fe–SiO_2 interaction existing in the silica-prompted iron catalysts could effectively stabilize the active phases and finally improves the stability of the catalysts [2,3,5]. However, unfortunately, this interaction enables the formation of metastable FeO_x and irreducible iron (II) silicate, which restrains the reduction and carburization of the catalyst and subsequently results in lower activity [1,3]. In addition, silica has an apparent impact on the hydrocarbon selectivity of iron catalyst because of the interactions of potassium and/or iron with supports [3,6].

The activity of silica-prompted iron catalysts can be upgraded by an enhanced degree of reduction and carburization. This is usually attained by the incorporation of chemical promoters such as Cu [7] and K [8,9]. Also, reduction and carburization ability can be improved by weakening the strong Fe–SiO_2 interaction, but this weakened interaction would pay a penalty in catalyst stability. Therefore, synergistic optimization between stability and activity by the modification of Fe–SiO_2 interaction becomes very important for the design of novel iron-based FTS catalysts. ZrO_2 is more chemically inert than classical supports such as SiO_2 and Al_2O_3 [10], and it is expected that the Fe–SiO_2 interaction would be modified by introducing ZrO_2 into SiO_2-promoted iron catalysts. However, few studies of this issue can be found in the literature. In contrast, much attention has been paid to improving the performance of Co/SiO_2 catalysts by modifying the Co–SiO_2 interaction via the incorporation of ZrO_2. Moradi et al. [11] report that the Co–SiO_2 interaction can be replaced by Co–Zr interaction by adding ZrO_2 in Co/SiO_2 catalysts, which favors the reduction of the catalysts. Moreover, the activity and selectivity toward higher hydrocarbons of the Zr-modified catalysts increased with increased ZrO_2 loading. Ali et al. [12] investigated the influence of ZrO_2 on the FTS performance over the sequentially impregnated Co/Zr/SiO_2 catalyst and found that both the activity and selectivity were improved due to the active interface between Zr and Co that could facilitate CO dissociation. Also, Jongsomjit et al. [13] studied Co dispersed on a mixed nano-SiO_2–ZrO_2 support and concluded that the number of active Co metal atoms increased due to the weakened Co–support interaction. More recently, researchers found that the modification of Co/MCM-41 catalysts by ZrO_2 weakened the Co–SiO_2 interaction, thus reducing the formation of hardly reducible cobalt species such as Co_2SiO_4 [14].

* Corresponding author at: State Key Laboratory of Coal Conversion, Institute of Coal Chemistry, Chinese Academy of Sciences, Taiyuan 030001, People's Republic of China. Fax: +86 351 7560835.
E-mail address: yyong@sxicc.ac.cn (Y. Yang).

0021-9517/$ - see front matter © 2011 Elsevier Inc. All rights reserved.
doi:10.1016/j.jcat.2011.01.005

The present study attempts to modify the Fe–SiO_2 interaction with ZrO_2 for iron-based FTS catalysts. A series of Fe/SiO_2 catalysts with different ZrO_2 content were designed and prepared by a precipitation method. The catalysts were characterized by N_2 adsorption, Fourier transform infrared spectroscopy (FTIR), X-ray photoelectron spectroscopy (XPS), H_2 temperature-programmed reduction (H_2-TPR), powder X-ray diffraction (XRD), transmission electronic microscopy (TEM), and Mössbauer effect spectroscopy (MES). The FTS performance of catalysts was tested in a fixed-bed reactor and correlated with the characterization results.

2. Experimental

2.1. Catalyst preparation

The catalyst precursors used in this study were prepared by a coprecipitation method. A solution containing $Fe(NO_3)_3$ (99.9+%; Tianjin Chemical Co., People's Republic of China), zirconium nitrate, and silica sol (SiO_2, 30.0 wt.%; Qingdao Ocean Chemical Co., People's Republic of China) with an Fe/SiO_2/ZrO_2 weight ratio of 100/20/x (x = 0, 1, 2, 5, 10, 20, 40) was mixed and then introduced into a 5-L precipitation vessel at 80 ± 1 °C. An NH_4OH solution (Tianjin Chemical Co.) was added simultaneously into this precipitation vessel to maintain the pH at a constant value of 8.5 ± 0.3. The obtained precipitate was completely washed with hot deionized water and then filtered. After that, the catalyst precursors were dried at 120 °C for 12 h, followed by calcination at 500 °C for 5 h in air. In this study, the catalysts containing different levels of ZrO_2 were denoted as Zr1, Zr2, Zr5, Zr10, Zr20, and Zr40 (with the ZrO_2 weight percentage varied from 1 to 40 per 100 Fe), respectively. The detailed catalyst composition and nomenclature are summarized in Table 1.

2.2. Catalyst handling and samples prepared for characterization

The reduced catalyst samples used for Mössbauer characterization were prepared by reducing the fresh catalysts in a quartz tube with synthesis gas (H_2/CO = 2.0) at 280 °C, 1000 h^{-1} GHSV, and 0.1 MPa for 24 h. After reduction, the sample was coated with paraffin wax to prevent oxidation.

One method was developed to study the stability of iron carbides, which includes the following steps: first, the fresh catalysts were carburized with synthesis gas (H_2/CO = 2.0) at 300 °C, 10,000 h^{-1} GHSV, and 0.1 MPa for 20 h. The obtained samples were coated with liquid wax and subsequently characterized by low-temperature MES to measure the iron carbide content. Second, the above process was conducted again. After activation, the samples were flushed with high-purity Ar (99.99+%) and then treated with an oxidation agent (3% H_2O/97% Ar) at 320 °C, 20,000 h^{-1} GHSV, and 0.1 MPa for 1.5 h. The obtained samples were also coated with liquid wax for low-temperature MES characterization. The oxidation degree was calculated based on the difference in iron carbide content of the sample, as defined in the text.

Table 1
The composition and textural properties of the zirconia-promoted FeSi catalysts as prepared.

Catalysts	Catalyst composition (parts by weight)	BET surface area[a] (m^2/g)	Pore volume[a] (cm^3/g)	Average pore size[a] (nm)
FeSi	100Fe/20SiO_2	222	0.53	7.8
Zr1	100Fe/20SiO_2–1ZrO_2	221	0.56	8.3
Zr2	100Fe/20SiO_2–2ZrO_2	223	0.61	8.9
Zr5	100Fe/20SiO_2–5ZrO_2	228	0.62	8.9
Zr10	100Fe/20SiO_2–10ZrO_2	232	0.57	8.0
Zr20	100Fe/20SiO_2–20ZrO_2	221	0.49	7.8
Zr40	100Fe/20SiO_2–40ZrO_2	217	0.44	7.1
FeZr	100Fe/20ZrO_2	57	0.25	13.0
α-Fe_2O_3	–	25	0.16	29.3

[a] Max error = ±5%.

2.3. Catalyst characterization

The textural properties of fresh catalysts were determined via N_2 physisorption at −196 °C, using a Micromeritics ASAP 2420 instrument. Each sample was degassed under vacuum at 90 °C for 1 h and 350 °C for 8 h prior to the measurement.

XRD measurements were carried out using a D/max-RA X-ray diffractometer (Rigaku, Japan) with Cu Kα radiation (λ = 0.154 nm) operated at 40 kV and 100 mA. The crystal phase compositions of the samples were determined by comparing the measured d-spacings with standard ASTM values. Silicon was used as an internal standard for correction of the angles derived from the diffraction lines and of the instrumental broadening for the crystallite size and cell parameter determination.

High-resolution transmission electronic microscopy (HRTEM) was performed on a JEOL 2010 HRTEM (JEOL, Japan) using an accelerating voltage of 200 kV. The calcined catalysts were dispersed in ethanol and mounted on a carbon foil supported on a copper grid.

The Mössbauer spectra of catalyst samples were obtained on an MR-351 constant-acceleration Mössbauer spectrometer (FAST, Germany) at room temperature and/or 20 K, using 25 mCi ^{57}Co in a Pd matrix. The spectrometer was operated in a symmetric constant-acceleration mode. The spectra were collected over 512 channels in the mirror image format.

The IR spectra were recorded with a Vertex 70 (Bruker) FTIR spectrophotometer. Powdered samples were diluted with KBr and pressed into translucent disks at room temperature. All spectra were taken in the range 4000–400 cm^{-1} at a resolution of 4 cm^{-1}.

XPS was recorded with a VG MultiLab 2000 system at a base pressure of 1×10^{-9} mbar. Samples were excited with monochromatized Al Kα radiation ($h\nu$ = 1486.6 eV). The analyzer was operated in a constant-pass-energy mode (20 eV). The C1s peak of adventitious carbon (284.6 eV) was used as a reference for estimating the binding energy. The binding energies were given with an accuracy of ±0.1 eV.

H_2-TPR was carried out using a dynamic analyzer (Micromeritics, Model 2920). About 40 mg of catalyst was treated in 10% H_2/90% Ar (v/v) (flow rate 50 ml/min), and the reduction temperature was increased from room temperature to 800 °C at a heating rate of 10 °C/min. The hydrogen consumption was calibrated using the H_2-TPR of CuO (Aldrich, 99.99+%) as the standard sample under the same conditions.

2.4. FTS performance

The FTS performance of the catalysts was tested in a stainless steel fixed-bed reactor with inner diameter of 12 mm. A quantity of 5 ml of catalyst was loaded into the reactor for all the reaction tests. The remaining volume of the reactor tube was filled with quartz granules in a size range of 20–40 mesh. All the catalysts were activated with syngas (H_2/CO = 2.0) at 280 °C, 0.10 MPa, and 1000 h^{-1} for 24 h. The reaction conditions were maintained at 270 °C, 1.5 MPa, 2000 h^{-1}, and H_2/CO = 2.0. A detailed description of the reactor and the product analysis system has been provided elsewhere [15].

3. Results and discussion

3.1. BET surface area

Table 1 gives the results of N_2 physisorption for the catalysts. Much higher BET surface areas (217–232 m^2/g) were found for

the catalysts containing SiO_2 than for the catalyst promoted only with ZrO_2. The BET surface areas of the SiO_2-promoted catalysts were essentially identical within experimental error. However, the BET surface area of the FeZr sample is only 57 m^2/g, which is slightly higher than that of α-Fe_2O_3. The above results implied that SiO_2 plays the critical role in determining the dispersion state of the iron oxides. It is known that ZrO_2 has a much weaker dispersion effect than SiO_2; therefore, it is understandable that the textural properties underwent much smaller changes when ZrO_2 was added into the SiO_2-promoted samples.

3.2. Interaction among Fe, O, Si, and Zr

3.2.1. Formation of Fe–O–Si interaction

As far as we know, direct evidence of Fe–SiO_2 interaction is scarcely reported, although this interaction has been extensively studied in iron-based FTS catalysts [16,17]. Fortunately, the asymmetric Si–O–Si stretching vibration of SiO_2 can easily be observed by FTIR spectroscopy. It is expected that this stretching mode would be disturbed if some interaction existed between iron and SiO_2. Thus, the study of the Si–O–Si asymmetric stretching vibration of SiO_2-promoted iron catalysts may shed light on the details of Fe–SiO_2 interaction.

Fig. 1 illustrates the FTIR spectra of FeSi samples at different preparation stages, and the typical frequency values and assignments are summarized in Table 2 [18,19]. The bands assigned to the vibration modes of NO_3^-, H_2O, NH_3^+, and CO_2 have not been discussed here. As can be seen, no obvious difference of the asymmetric Si–O–Si stretching vibration centered at 1120 cm^{-1} was discerned when SiO_2 sol was mixed with Fe $(NO_3)_3$ solution, indicating that SiO_2 and iron existed in their original state (see spectra a, b, and c in Fig. 1). In the sample after precipitation (see spectrum d in Fig. 1), the Si–O–Si asymmetric stretching vibration peak shifted slightly to lower wavenumber. It is known that iron oxyhydroxides were formed after precipitation and that a large percentage of Fe ions were at coordinate unsaturated sites (CUS), which may be incorporated with SiO_2 to form Fe–O–Si complexes [20]. This weak interaction disturbed the Si–O–Si structure slightly. In the dried sample (see spectrum e in Fig. 1), the Si–O–Si vibration peak disappeared, while a strong peak at 1000 cm^{-1} was obviously observed. As illustrated in Fig. 2 [20,21], when the precipitate was exposed to thermal treatment, H_2O was gradually removed and the

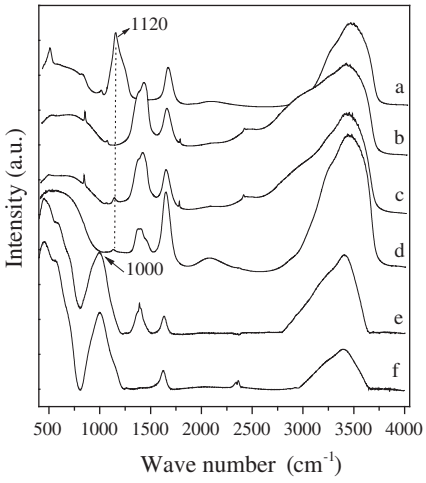

Fig. 1. FTIR spectra of FeSi sample at different preparation stages of (a) SiO_2 sol, (b) Fe $(NO_3)_3$ solution, (c) mixed solution of SiO_2 sol and Fe $(NO_3)_3$, (d) after precipitation, (e) after drying at 120 °C for 12 h, and (f) after calcination at 500 °C for 5 h.

Table 2
IR frequencies (cm^{-1}) and assignments.

Frequencies (cm^{-1})	Assignment
3440	$\upsilon(H_2O)$
1624	$\delta(H_2O)$
2400	$\upsilon_{as}(CO_2)$
2078	$\upsilon_s(NH_3^+)$
1421	$\upsilon_{as}(NO_3^-)$
851	$\upsilon(NO_3^-)$
1113, 1070	υ_{as}(Si–O–Si) in solid state
1120	υ_{as}(Si–O–Si) in sol state
803	υ_s(Si–O–Si)
474	δ(O–Si–O)
539	υ(Fe–O)
470	υ(Fe–O)

Fe–O–Si complex was strengthened to form an Fe–O–Si structure. It is reasonable that the reduced mass of the Si–O–Si harmonic oscillator will be increased when the Fe atom is substituted for Si since the atomic weight of iron is greater than that of silicon. Consequently, the asymmetric stretching vibration of Si–O–Si at 1113 cm^{-1} shifted to lower values [22], and the peak at 1000 cm^{-1} can be assigned safely to the Fe–O–Si bond [18,23–25]. Therefore, the Fe–SiO_2 interaction could be explained in terms of the formation of Fe–O–Si bonds between iron oxyhydroxides and SiO_2 during the drying process, and this structure still existed in the calcined sample (see spectrum f in Fig. 1). Due to the formation of this interaction, particle agglomeration to form large iron oxides particle was restrained, which resulted in a high-dispersion state of iron oxides. This may be the origin of the strong dispersion effect of the SiO_2 matrix. As a result, the characteristic stretching vibration bands of Fe–O bonds in FeSi catalysts, centered at 470 and 539 cm^{-1}, became broad and less intensive [26,27] (see Fig. 3a). As expected, there was no significant change in the FTIR spectrum of FeZr catalyst compared with that of α-Fe_2O_3, indicating that the Fe–ZrO_2 interaction is relatively weak [28,29].

The XPS spectra of Fe2*p*, Si2*p*, O1*s*, and Zr3*d* for the fresh catalysts are shown in Fig. 4a-d, respectively. The binding energies are listed in Table 3. It should be noted that all the O1*s* spectra can be fitted with two lines except for the pure SiO_2 sample. In the iron-containing samples, the lower values of O1*s* binding energies were assigned to O atoms close to Fe cations [30] ($O_{Fe}1s$), and the higher ones can be assigned to either O atoms close to Si cations or O atoms in the adsorbed OH on the surface of the catalysts [30,31].

Comparing FeSi with α-Fe_2O_3, the binding energy of Fe2*p* obviously shifted to higher value (see Fig. 4a). A similar trend of the $O_{Fe}1s$ binding energy was observed in Fig. 4b. The shift in core-level binding energy is caused by the variation of the electron density around the central atom. It is known that the electron density of the central atom is greatly influenced by the electronegativity of the atoms surrounded; namely, the greater the electronegativity of the adjacent atoms (groups), the lower the electron density of the central atom due to partial electron transfer [32]. The binding energy shift of Fe2*p*, Si2*p*, and $O_{Fe}1s$ indicated that the electron density of Fe–O_{Fe} units and Si changed relative to their pure oxides. As concluded above, an Fe–O–Si structure was formed in FeSi samples, indicating that the Fe–O_{Fe} units were surrounded by Si species. It is reasonable that the electron density of Fe–O_{Fe} units would decrease since the electronegativity of Si^{4+} is much higher than that of Fe^{3+} [33,34]. This resulted in an electron-deficient state of Fe–O_{Fe} units and an electron-rich state of Si species. Consequently, the binding energies of Fe2*p* and $O_{Fe}1s$ increased, while the Si2*p* binding energy decreased, relative to their respective pure oxides [31]. (A detailed discussion of the shifts of binding energy can be found in the Supporting information.)

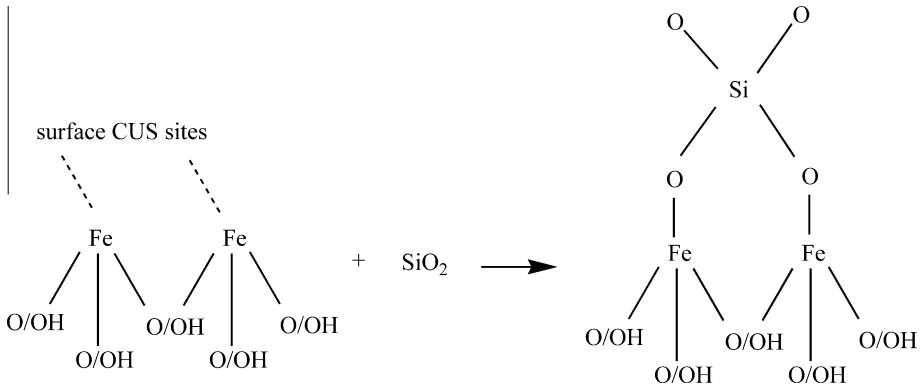

Fig. 2. Proposed model for Fe–O–Si species formation.

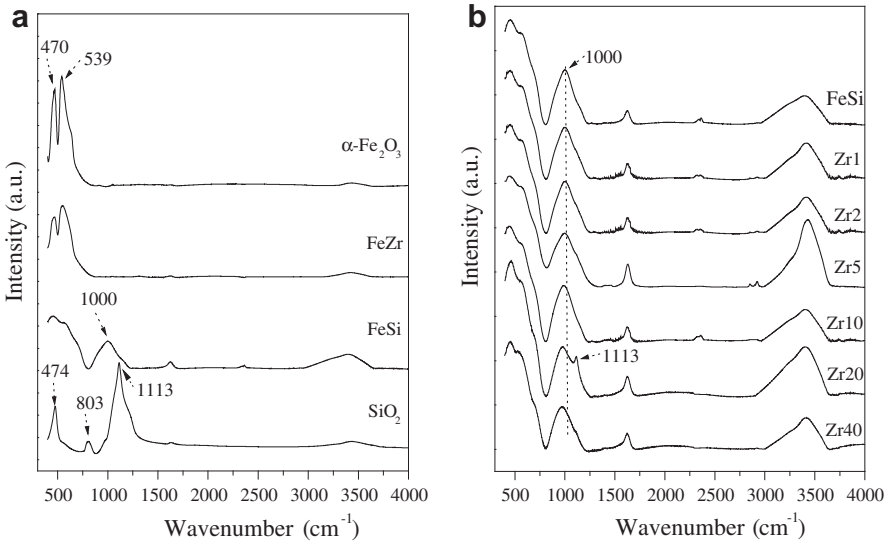

Fig. 3. FTIR spectra of the zirconia-promoted FeSi catalysts as prepared.

3.2.2. Modification of Fe–O–Si interaction

Fig. 3b shows the FTIR spectra of ZrO_2-modified FeSi catalysts. It is obvious that the band at 1000 cm^{-1} shifted gradually to lower wavenumber with increasing ZrO_2 content. A possible explanation for this observation is given below.

In the present study, Zr^{4+}, Fe^{3+}, and SiO_2 sol were mixed and precipitated together; it must be born in mind that Fe^{3+} cations precipitate at a lower pH value than Zr^{4+}. Therefore, the Fe^{3+} cations precipitate earlier than the Zr^{4+} cations. Thus, the formation of iron oxyhydroxide particles surrounded by a layer of Zr oxide precursor is a reasonable scenario. These Zr oxide precursors may act as a protecting layer between iron oxyhydroxides and SiO_2. With increasing ZrO_2 content, more sites on the iron oxyhydroxides that directly interacted with SiO_2 were covered; thus, the amount of Fe–O–Si structure was reduced. Moreover, the formation of Si–O–Zr linkage could not be ignored since this structure has frequently been observed in ZrO_2–SiO_2 mixed materials [35–37]. In other words, the Fe–SiO_2 interaction is effectively weakened by ZrO_2. If one accepts the postulate above, then the redshift of the bands at 1000 cm^{-1} would be expected because the wavenumber of Zr–O–Si linkages is considered to be lower than that of Fe–O–Si (1000 cm^{-1}) [37–39]. One may note that a shoulder peak appeared at 1113 cm^{-1} in the Zr20 sample, coinciding with the asymmetric stretching vibration of Si–O–Si. This indicates that part of SiO_2 did not interact with iron in this sample.

The binding energies of Fe2*p*, Si2*p*, O1*s*, and Zr3*d* changed obviously due to the modification of Fe–SiO_2 interaction by ZrO_2, as shown in Fig. 4a–d and Table 3. Specifically, both the binding energies of Fe2*p* and O_{Fe}1*s* relative to that of FeSi catalysts decreased gradually with the addition of ZrO_2, suggesting that the electron transfer via the Fe–O–Si structure was disturbed. Reasons for this phenomenon cannot be clearly understood due to the complex catalyst composition but may be related to the fact that the charge was redistributed, since the amount of Fe–O–Si structure was decreased by the addition of ZrO_2. This hindered the partial electron transfer from Fe–O_{Fe} units to Si species via Fe–O–Si bonds. Thus, the binding energies of both Fe2*p* and O_{Fe}1*s* decreased slightly. A Zr–O–Si linkage could be formed when the ZrO_2 content was high enough, as demonstrated earlier. If this was the case, the electron density of Zr–O units would decrease, because the electronegativity of Zr^{4+} is lower than that of Si^{4+} [33,34]. This effect shifted the binding energy of Si2*p* to lower values, especially for the Zr40 sample, as evidenced in Fig. 4c. And the binding energy of Zr3*d* increased accordingly compared to that of pure ZrO_2 (shown in Fig. 4d). Similarly, Bosman et al. [31]observed an increase in Zr3*d* binding energy and a decrease in Si2*p* binding energy in the coprecipitated

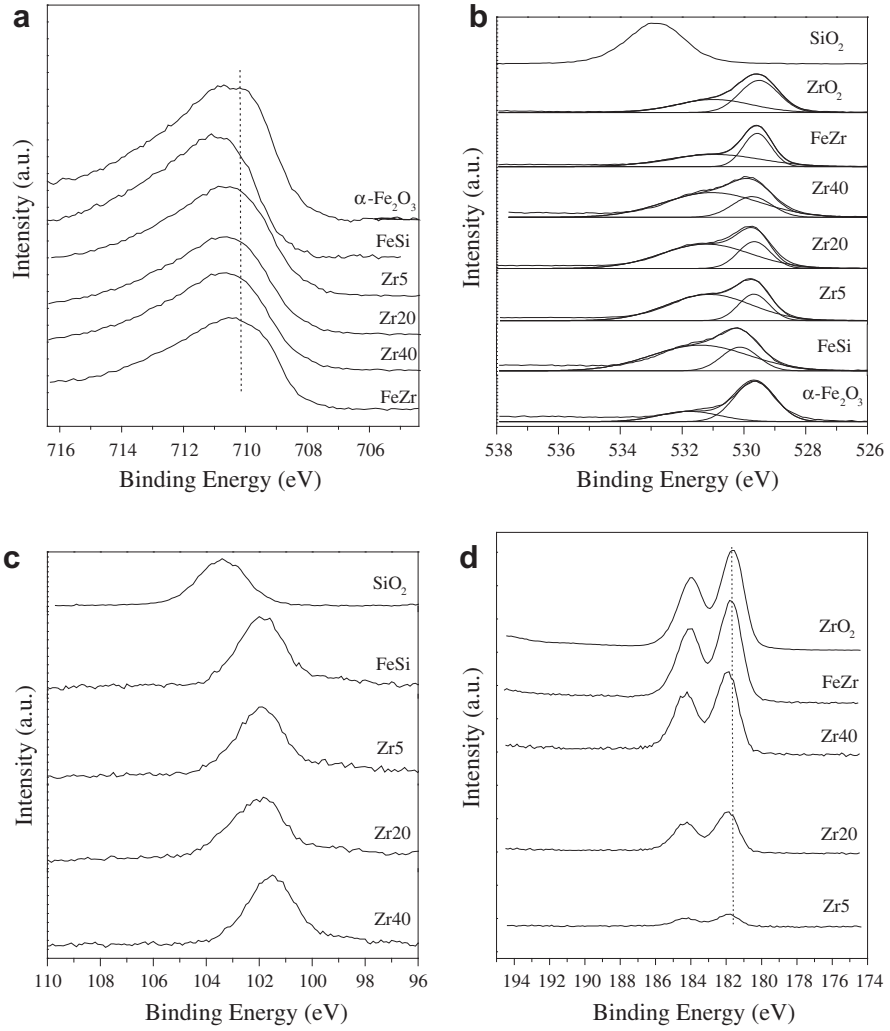

Fig. 4. (a) Fe2*p*, (b) O1*s*, (c) Si2*p*, and (d) Zr3*d* XPS spectra of the zirconia-promoted FeSi catalysts as prepared.

Table 3
Binding energies of XPS lines of the zirconia-promoted FeSi catalysts as prepared.

Catalysts	Binding energy[d] (eV)					M/Fe[e] (×10² atomic ratio)				Surface/bulk	
	Fe2p	O_{Fe}1s[a]	O1s[b]	Zr3d	Si2p	Bulk (ICP)		Surface (XPS)			
						Si/Fe	Zr/Fe	Si/Fe	Zr/Fe	Si/Fe	Zr/Fe
α-Fe_2O_3	710.7	529.6	531.7	–	–	–	–	–	–	–	–
FeSi	711.1	530.1	531.4	–	102.0	18.3	–	28.8	–	1.6	–
Zr5	710.8	529.7	531.2	181.7	101.8	17.8	2.1	33.2	3.4	1.9	1.6
Zr20	710.5	529.6	531.3	181.8	101.8	17.2	8.8	34.0	13.9	2.0	1.6
Zr40	710.6	529.7	531.1	181.8	101.5	17.3	17.9	34.8	28.5	2.0	1.6
FeZr	710.5	529.5	531.1	181.7	–	–	8.7	–	35.3	–	4.1
ZrO_2	–	529.5[c]	530.9	181.6	–	–					
SiO_2	–	–	533.0	–	103.3	–					

[a] The oxygen close to the Fe atom.
[b] The oxygen close to the Si atom or the oxygen in OH.
[c] The oxygen close to the Zr atom.
[d] Max error = ±0.1 eV.
[e] Max error = ±3%.

mixed ZrO_2–SiO_2 samples. As for FeZr samples, the Fe2*p*, O_{Fe}1*s*, and Zr3*d* binding energies were similar to those of their pure oxides, implying that the Fe–ZrO_2 interaction is relatively weak. It should be noted that the O1*s* binding energies with higher values (531.2 ± 0.2 eV) are not discussed here since they can be ascribed either to the oxygens near Si cations or to the adsorbed OH. Table 3 presents the surface compositions of the catalysts. As can be seen, the surface Zr/Fe atomic ratio was much higher than that in the bulk due to the fact that Fe^{3+} cations precipitate earlier than Zr^{4+} cations. For catalysts containing ZrO_2 and SiO_2, both the Si/Fe and Zr/Fe atomic ratios were higher than those of the bulk, indicating that Si and Zr are enriched on the surface of catalysts simultaneously.

3.3. Reduction behavior of the catalysts

The reduction behaviors of the catalysts were measured by H_2-TPR. The reduction profiles and H_2 consumption for the catalysts are presented in Fig. 5 and Table 4, respectively. Both the

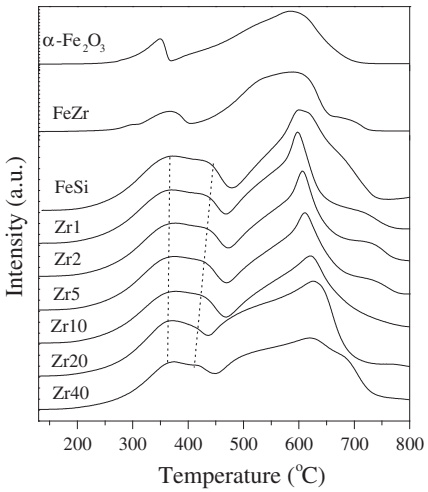

Fig. 5. H_2-TPR profiles of the zirconia-promoted FeSi catalysts.

Table 4
Quantitative results of H_2 consumption for the zirconia-promoted FeSi catalysts in H_2-TPR.[a,b]

Catalysts	Peak	Peak center	H_2 consumption (mol H_2/mol Fe)
α-Fe_2O_3	I	345	0.15
	II	508	0.52
	III	598	0.76
FeZr	I	358	0.15
	II	496	0.35
	III	584	0.92
FeSi	I	373	0.47
	II	432	0.05
	III	608	0.60
Zr2	I	372	0.39
	II	433	0.04
	III	553	0.22
	IV	609	0.23
	V	671	0.25
Zr5	I	371	0.40
	II	430	0.02
	III	537	0.24
	IV	610	0.24
	V	689	0.23
Zr10	I	368	0.40
	II	428	0.01
	III	534	0.23
	IV	615	0.33
	V	679	0.18
Zr20	I	367	0.34
	II	411	0.01
	III	514	0.35
	IV	627	0.40
	V	766	0.09
Zr40	I	365	0.33
	II	420	0.01
	III	505	0.35
	IV	627	0.48
	V	799	0.03

[a] The H_2 consumption was measured from the area under the corresponding peak.
[b] Max error = ±2%.

α-Fe_2O_3 and FeZr catalysts exhibited the typical two-step reduction process of hematite, i.e., α-Fe_2O_3 → Fe_3O_4 → α-Fe [2,40]. This was verified by the amount of H_2 consumption (0.15 mol H_2/mol Fe for the lower-temperature reduction peak and 1.28 mol H_2/mol Fe for the higher-temperature one). However, the first reduction peak of α-Fe_2O_3 (345 °C) was lower than that of FeZr sample (358 °C). As mentioned above, ZrO_2 enriched on the surface of FeZr sample may cover part of the Fe sites and as a result restrain the reduction of α-Fe_2O_3 to Fe_3O_4.

All the SiO_2-promoted catalysts exhibited two main broadened reduction regions. The onset of the first region was apparently retarded compared to that of α-Fe_2O_3, and this region was well fitted with two peaks (peaks I and II). The peak assignment can be made by calculating the H_2 consumption of the peaks (validated by the results of H_2-DTG, see Supplementary information, Table S1). For FeSi catalyst, peak I should be ascribed to the reduction of α-Fe_2O_3 to Fe_3O_4 and part of Fe_3O_4 to Fe^{2+} species, and peak II may be composed of the reduction of the remainder of Fe_3O_4, which strongly interacted with SiO_2 to Fe^{2+} species. The sum of H_2 consumption for peaks I and II (0.52 mol H_2/mol Fe), consistent with the theoretical value of Fe^{3+} to Fe^{2+} (0.5 mol H_2/mol Fe), verified the above statement. These Fe^{2+}/Si compounds can be present in the form of either wüstite (FeO) or Fe_2SiO_4, which cannot be reduced completely even at high temperature [2,41]. Thus, the total H_2 consumption (1.12 mol H_2/mol Fe) was significantly lower than that of theoretical α-Fe_2O_3 → α-Fe (1.5 mol H_2/mol Fe). Researchers usually ascribe this reduction behavior of FeSi catalysts to the Fe–SiO_2 interaction. But the intrinsic mechanism for this phenomenon is still in controversy. In the present study, the formation of Fe–O–Si bonds between iron oxide and SiO_2 was observed. Moreover, the XPS results further demonstrated that the electron density of Fe–O_{Fe} units was decreased, leading to an electron-deficient state of the Fe valence level. It means that more core-level electron of Fe nuclei took part in Fe–O_{Fe} bonds, which strengthened the Fe–O_{Fe} bonds and made the removal of oxygen difficult during reduction or activation.

Fig. 5 shows that the first reduction region gradually shifted to lower temperature with increasing ZrO_2 content. Based on the fitting results, both the reduction temperature and the H_2 consumption amount of the first two fitted peaks decreased with increasing ZrO_2 content, which was more obvious for peak II. These results suggested that the reduction of α-Fe_2O_3 to Fe_3O_4 and Fe_3O_4 to Fe^{2+} species was promoted by ZrO_2 and that the amount of Fe_3O_4 that strongly interacted with SiO_2 was reduced. As confirmed by FTIR and XPS, the Fe–SiO_2 interaction can be effectively weakened by ZrO_2. It is generally accepted that Fe^{2+} species (FeO or Fe_2SiO_4) can only be stabilized where Fe–SiO_2 interaction is strong [2,41]. Thus, not all the α-Fe_2O_3 particles were reduced to Fe^{2+} species during the first reduction process because of the weakened Fe–SiO_2 interaction, which resulted in reduced H_2 consumption. Moreover, the weakened Fe–SiO_2 interaction facilitated the reduction of α-Fe_2O_3 to Fe_3O_4 and Fe_3O_4 to Fe^{2+} species, shifting the reduction temperature of peaks I and II to lower values.

It should be noted that the high-temperature reduction regions of the SiO_2-containing catalysts can be tentatively fitted with several peaks. These peaks can be ascribed to the reductions of Fe_3O_4 and Fe^{2+} species interacted with SiO_2 with different strength to α-Fe. It is apparent that the total H_2 consumption increased slightly with increasing ZrO_2 content, suggesting that the reduction degree was improved.

3.4. Crystalline structure of the catalysts

The crystalline structure of the fresh catalysts was measured by MES at room temperature and XRD. Due to the highly dispersed state of the catalysts caused by the strong dispersion effect of silica

[2,3], MES measured at room temperature cannot give the detailed phase composition (see Tables S2 and S3). Thus, the crystalline structures of the reduced and used samples were measured by MES at 20 K.

3.4.1. Catalysts samples as prepared

XRD patterns (see Supporting information, Fig. S4) show that iron phases in FeZr and α-Fe_2O_3 catalysts as prepared are well-crystallized hematite with characteristic diffraction peaks at 2θ angles of 24.2°, 33.1°, 35.6°, 40.8°, 49.52°, 54.0°, 57.6°, 62.5°, and 64.0°. In contrast, all the SiO_2-containing catalysts show two broad diffraction regions around 35° and 63.5°, which is characteristic of amorphous iron oxide with various crystallite diameters lower than 4–5 nm [42]. Fig. 6 illustrates the Mössbauer spectra of the fresh catalysts recorded at room temperature. The spectral parameters are given in Table 5. The FeZr catalyst showed one sextet, very similar to that of α-Fe_2O_3. This sextet can be assigned to the ferromagnetic α-Fe_2O_3 with particle size larger than 13.5 nm [9,43–46]. For the catalysts incorporated with SiO_2, the sextet disappears and only the doublet is present. The Mössbauer parameters of the doublets were typical of superparamagnetic Fe^{3+} irons on the noncubic sites with crystallite diameters less than 13.5 nm [44,46–50]. These results indicated that the particle size of SiO_2-containing catalysts was smaller than those of FeZr and α-Fe_2O_3. Based on detailed study of the particle size distribution by TEM (see Supporting information, Figs. S5 and S6), all the SiO_2-containing catalysts showed almost the same average particle size, in the range 5–7 nm. The above analysis showed that ZrO_2 has little influence on the dispersion state of the iron oxides containing SiO_2, which was governed by strong dispersion effect of SiO_2. This observation is consistent with the results of BET analysis.

3.4.2. Catalyst samples after reduction

Fig. 7 presents the Mössbauer spectra of the reduced catalysts measured at 20 K. All the Mössbauer patterns can be fitted with five sextets, representing Fe_3O_4 and iron carbides with different hyperfine parameters [30,51]. The fitting results are summarized in Table 6. As can be seen, the increase in ZrO_2 loading led to an increase in Fe_5C_2 content, indicating that ZrO_2 enhanced the reduction and carburization ability of catalysts. It has been frequently reported that the carburization ability of SiO_2-containing catalysts is restrained by the strong Fe–SiO_2 interaction [2,3]. In the present study, the strong Fe–SiO_2 interaction was effectively weakened by ZrO_2; thus, the reduction and carburization ability of catalysts were improved. As expected, the Fe_5C_2 content in reduced FeZr catalyst was close to that of α-Fe_2O_3, consistent with the fact that the Fe–ZrO_2 interaction is relatively weak, which guaranteed the easier reduction and carburization of FeZr catalysts.

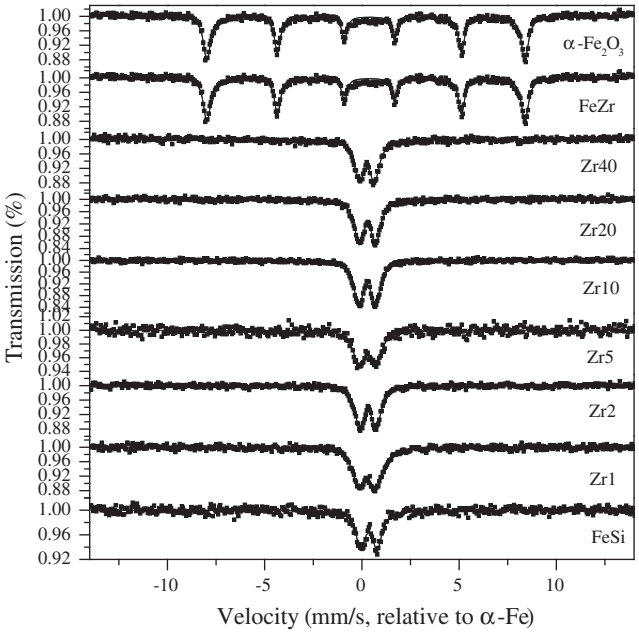

Fig. 6. Mössbauer spectra of the zirconia-promoted FeSi catalysts as prepared, measured at room temperature.

Table 5
Mössbauer parameters of the zirconia-promoted FeSi catalysts obtained at room temperature as prepared.

Catalysts	Phases	IS (mm/s)	QS (mm/s)	Hhf (kOe)	Area[a] (%)	d_p (nm)
FeSi	Fe^{3+} (spm)	0.36	0.86		100	<13.5
Zr1	Fe^{3+} (spm)	0.30	0.88		100	<13.5
Zr2	Fe^{3+} (spm)	0.31	0.85		100	<13.5
Zr5	Fe^{3+} (spm)	0.30	0.88		100	<13.5
Zr10	Fe^{3+} (spm)	0.30	0.88		100	<13.5
Zr20	Fe^{3+} (spm)	0.29	0.86		100	<13.5
Zr40	Fe^{3+} (spm)	0.29	0.83		100	<13.5
FeZr	α-Fe_2O_3	0.30	−0.18	509	100.0	>13.5
α-Fe_2O_3	α-Fe_2O_3	0.30	−0.15	513	100.0	>13.5

[a] Max error = ±1%.

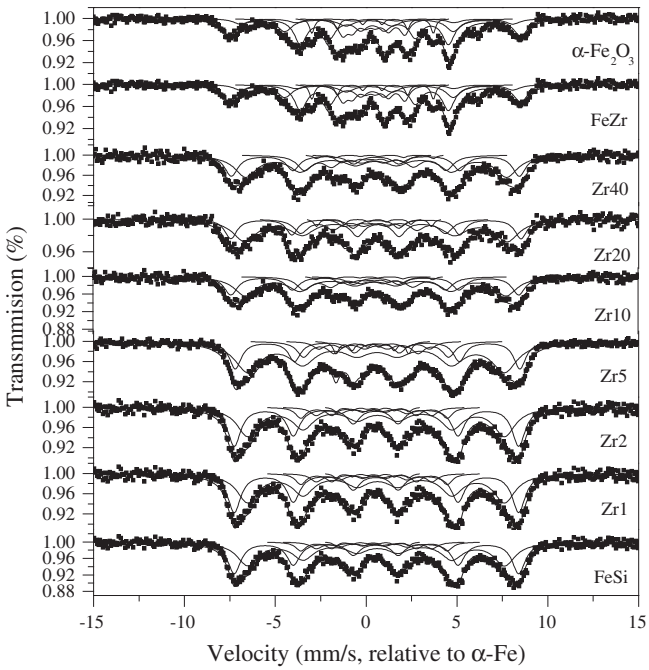

Fig. 7. Mössbauer spectra of the zirconia-promoted FeSi catalysts after reduction, measured at 20 K.

3.4.3. Catalyst samples after FTS reaction

Fig. 8 shows the Mössbauer spectra measured at 20 K of the catalysts after FTS reaction. They can also be fitted with five sextets with different hyperfine parameters [30,51]. As summarized in Table 7, the used catalysts were composed of Fe_3O_4 and χ-Fe_5C_2 with different ratios. It is found that the iron carbide content in the used catalysts increased with the increasing ZrO_2 content except Zr40. For all the SiO_2-promoted catalysts, the χ-Fe_5C_2 content in the reduced catalysts increased to a certain extent during FTS reaction due to the further carburization. As for FeZr and α-Fe_2O_3 catalysts, however, the χ-Fe_5C_2 content decreased sharply from 44.5% and 50.4% after reduction to 5.8% and 6.5% after reaction, respectively. The explanation for these observations will be detailed later.

Table 6
Mössbauer parameters of the zirconia-promoted FeSi catalysts after reduction obtained at 20 K.[a,b]

Catalysts	IS (mm/s)	QS (mm/s)	Hhf (kOe)	Area[c] (%)	Assignment
FeSi	0.55	0.04	487	37.9	Fe_3O_4 (A)
	0.59	−0.08	440	44.9	Fe_3O_4 (B)
	0.43	0.00	251	8.4	χ-Fe_5C_2 (I)
	0.42	0.05	198	6.9	χ-Fe_5C_2 (II)
	0.37	−0.04	105	1.9	χ-Fe_5C_2 (III)
Zr5	0.55	−0.03	490	25.4	Fe_3O_4 (A)
	0.60	0.01	452	54.6	Fe_3O_4 (B)
	0.42	0.10	253	12.5	χ-Fe_5C_2 (I)
	0.41	0.10	207	5.0	χ-Fe_5C_2 (II)
	0.58	0.14	109	2.5	χ-Fe_5C_2 (III)
Zr10	0.51	0.04	497	23.1	Fe_3O_4 (A)
	0.61	−0.05	450	52.3	Fe_3O_4 (B)
	0.55	0.00	252	13.6	χ-Fe_5C_2 (I)
	0.42	0.05	203	6.0	χ-Fe_5C_2 (II)
	0.37	−0.04	113	4.9	χ-Fe_5C_2 (III)
Zr20	0.53	−0.06	500	26.6	Fe_3O_4 (A)
	0.59	0.01	456	44.7	Fe_3O_4 (B)
	0.43	0.16	252	20.3	χ-Fe_5C_2 (I)
	0.34	0.29	200	2.2	χ-Fe_5C_2 (II)
	0.30	0.10	113	6.2	χ-Fe_5C_2 (III)
Zr40	0.54	0.00	500	23.0	Fe_3O_4 (A)
	0.60	−0.13	458	48.9	Fe_3O_4 (B)
	0.44	−0.10	251	18.5	χ-Fe_5C_2 (I)
	0.53	−0.20	199	3.7	χ-Fe_5C_2 (II)
	0.30	0.10	112	5.9	χ-Fe_5C_2 (III)
FeZr	0.54	−0.01	505	18.7	Fe_3O_4 (A)
	0.62	0.01	458	36.8	Fe_3O_4 (B)
	0.40	0.00	251	17.3	χ-Fe_5C_2 (I)
	0.31	0.00	199	15.8	χ-Fe_5C_2 (II)
	0.36	0.13	109	11.4	χ-Fe_5C_2 (III)
α-Fe_2O_3	0.55	−0.01	504	16.8	Fe_3O_4 (A)
	0.65	−0.01	459	32.8	Fe_3O_4 (B)
	0.45	0.09	252	20.5	χ-Fe_5C_2 (I)
	0.37	0.07	199	17.6	χ-Fe_5C_2 (II)
	0.36	0.13	109	12.3	χ-Fe_5C_2 (III)

[a] Reduction conditions: 280 °C, 0.1 MPa, H_2/CO = 2.0, 24 h, and GHSV = 1000 h^{-1}.
[b] The data of Zr1 and Zr2 have been omitted since they are very similar to those of FeSi.
[c] Max error = ±1%.

3.5. Stability of iron carbides

Under typical FTS conditions where H_2O is present, the iron carbides can be oxidized to Fe_3O_4, leading to the deactivation of the catalysts [52,53]. It is known that SiO_2 could stabilize the iron carbides due to the Fe–SiO_2 interaction, although it is not understood why it should [3,5]. As confirmed earlier, the Fe–SiO_2 interaction was weakened by ZrO_2. It is necessary to examine whether this weakened Fe–SiO_2 interaction could effectively stabilize the iron carbides. Table 8 summarizes the phase compositions of the catalysts before and after H_2O oxidation. It is apparent that the oxidation degree decreased gradually with increasing ZrO_2 loading, indicating that the stability of iron carbides was improved. However, this is not the case when ZrO_2 content is further increased to that in Zr40 catalyst, which suggests that too high ZrO_2 content is not desirable. For FeZr catalysts, the oxidation degree was close to that of α-Fe_2O_3, higher than that of catalysts containing SiO_2, implying that ZrO_2 cannot stabilize the iron carbides effectively.

The above results suggested that iron carbides were more stable against H_2O oxidation in ZrO_2-modified FeSi catalysts. This improved stability cannot be ascribed simply to the stabilization effect caused by ZrO_2. It could be true that the stability of iron carbides can be effectively improved on the mixed ZrO_2–SiO_2 materials caused by the synergistic effects when the ZrO_2/SiO_2 ratio is appropriate, although further investigation is needed to substantiate this hypothesis. This is consistent with the study of Feller et al. [54], where the resistance of Co species to reoxidation by H_2O was enhanced by incorporation of zirconia into Co/SiO_2 catalysts. For Zr40, more iron carbides would be oxidized by H_2O caused by the decoration of zirconia.

3.6. FTS performance

The FTS performance of the catalysts was measured under reaction conditions of 270 °C, 1.5 MPa, H_2/CO = 2.0, and GHSV = 2000 h^{-1}. The activity, stability, and product selectivity were tested within a period of about 200-h steady-state runs.

3.6.1. FTS performances of the catalysts

The effects of ZrO_2 addition on the FTS performances of FeSi catalysts are presented in Fig. 9a. CO conversion was used as a measure of FTS activity in the current study [3]. The results showed that FeZr catalysts exhibited higher initial activity but deactivated quickly with time on stream (TOS). In contrast, CO conversion of FeSi catalysts remained almost unchanged during the whole reaction period. It should be noted that the activities of all the ZrO_2-modified FeSi catalysts increased with TOS, except Zr1, which contained the lowest level of ZrO_2. Moreover, the activity increased with increasing ZrO_2 loading, reached a maximum for Zr20 catalyst, and then decreased with further increasing ZrO_2 content (Zr40 catalyst). According to the carbide model [55–57], the bulk carbide phase plays an important role in controlling the number

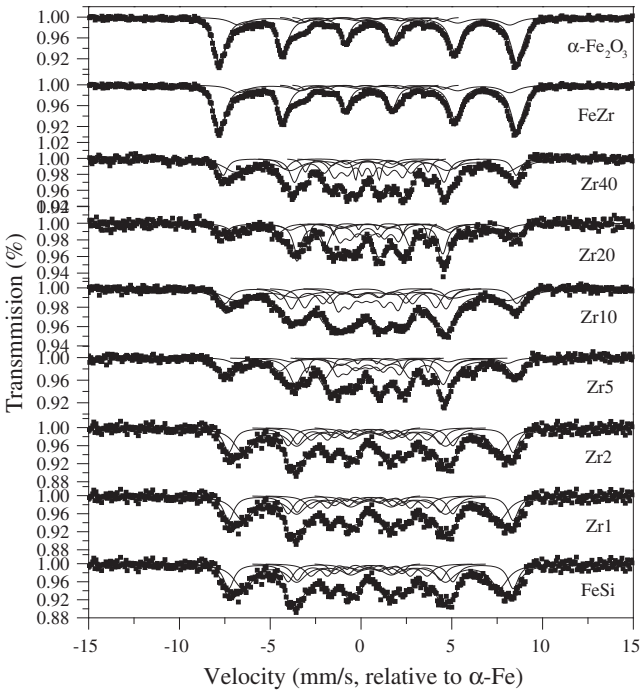

Fig. 8. Mössbauer spectra of the zirconia-promoted FeSi catalysts after the FTS reaction, measured at 20 K.

of active sites. Thus, the iron carbide content determined by MES can be used to monitor the number of active FTS sites to some extent. As stated above, the reduction and carburization degree of the catalysts were improved by ZrO_2. The observed increase in the activity with increasing ZrO_2 content in the present study is in good agreement with the characterization studies.

Fig. 9b compares the CO conversion and the iron carbide content at different stages of the selected catalysts. It is known that the interconversion between iron oxides and iron carbides is

Table 8
The phase evolution of the carburized catalysts during oxidation by H_2O.

Catalysts	Phase composition (after reduction)[a]		Phase composition (after oxidation)[a]		Oxidation degree (D%)[b]
	Fe_5C_2 (%)	Fe_3O_4 (%)	Fe_5C_2 (%)	Fe_3O_4 (%)	
FeSi	34.7	65.4	22.3	77.7	36
Zr1	40.3	59.7	26.8	73.2	33
Zr2	42.5	57.5	29.6	70.4	30
Zr5	44.6	55.4	32.2	67.8	28
Zr10	46.6	53.3	34.9	65.1	25
Zr20	49.0	51.0	36.3	63.6	25
Zr40	53.5	46.6	36.9	63.1	31
FeZr	100	0	59.3	40.6	41
α-Fe_2O_3	100	0	50.2	49.8	50

[a] Max error = ± 1%.
[b] $D\% = (A - B)/A \times 100\%$, where A = χ-Fe_5C_2 content after reduction; B = χ-Fe_5C_2 content after oxidation by H_2O.

Table 7
Mössbauer parameters of the zirconia-promoted FeSi catalysts after FTS reaction obtained at 20 K.[a,b]

Catalysts	IS (mm/s)	QS (mm/s)	Hhf (kOe)	Area[c] (%)	Assignment
FeSi	0.41	−0.05	485	33.2	Fe_3O_4 (A)
	0.64	0.09	439	33.8	Fe_3O_4 (B)
	0.47	0.14	245	16.6	χ-Fe_5C_2 (I)
	0.43	−0.02	200	11.8	χ-Fe_5C_2 (II)
	0.35	−0.12	112	4.7	χ-Fe_5C_2 (III)
Zr5	0.38	0.18	497	32.0	Fe_3O_4 (A)
	0.66	0.10	440	10.5	Fe_3O_4 (B)
	0.35	0.11	254	30.8	χ-Fe_5C_2 (I)
	0.30	−0.04	205	12.4	χ-Fe_5C_2 (II)
	0.30	0.10	109	14.4	χ-Fe_5C_2 (III)
Zr10	0.32	0.33	500	30.0	Fe_3O_4 (A)
	0.63	0.10	466	9.5	Fe_3O_4 (B)
	0.41	0.11	253	35.8	χ-Fe_5C_2 (I)
	0.35	0.01	208	8.2	χ-Fe_5C_2 (II)
	0.33	0.18	106	16.5	χ-Fe_5C_2 (III)
Zr20	0.31	0.25	503	19.9	Fe_3O_4 (A)
	0.60	0.10	465	17.7	Fe_3O_4 (B)
	0.44	0.12	252	35.5	χ-Fe_5C_2 (I)
	0.40	0.01	205	7.4	χ-Fe_5C_2 (II)
	0.40	0.10	107	19.5	χ-Fe_5C_2 (III)
Zr40	0.48	0.00	502	15.1	Fe_3O_4 (A)
	0.59	0.12	464	33.9	Fe_3O_4 (B)
	0.41	0.10	256	23.3	χ-Fe_5C_2 (I)
	0.43	0.06	210	9.3	χ-Fe_5C_2 (II)
	0.38	0.06	112	18.4	χ-Fe_5C_2 (III)
FeZr	0.45	0.00	507	29.0	Fe_3O_4 (A)
	0.63	−0.01	465	65.2	Fe_3O_4 (B)
	0.38	0.09	251	2.9	χ-Fe_5C_2 (I)
	0.36	0.00	201	2.9	χ-Fe_5C_2 (II)
α-Fe_2O_3	0.39	0.06	508	30.5	Fe_3O_4 (A)
	0.66	0.04	463	63.0	Fe_3O_4 (B)
	0.40	−0.10	251	3.5	χ-Fe_5C_2 (I)
	0.32	0.01	202	3.0	χ-Fe_5C_2 (II)

[a] Reaction conditions: 270 °C, 1.5 MPa, H_2/CO = 2.0, and GHSV = 2000 h^{-1}.
[b] The data of Zr1 and Zr2 have been omitted since they are very similar to those of FeSi.
[c] Max error = ±1%.

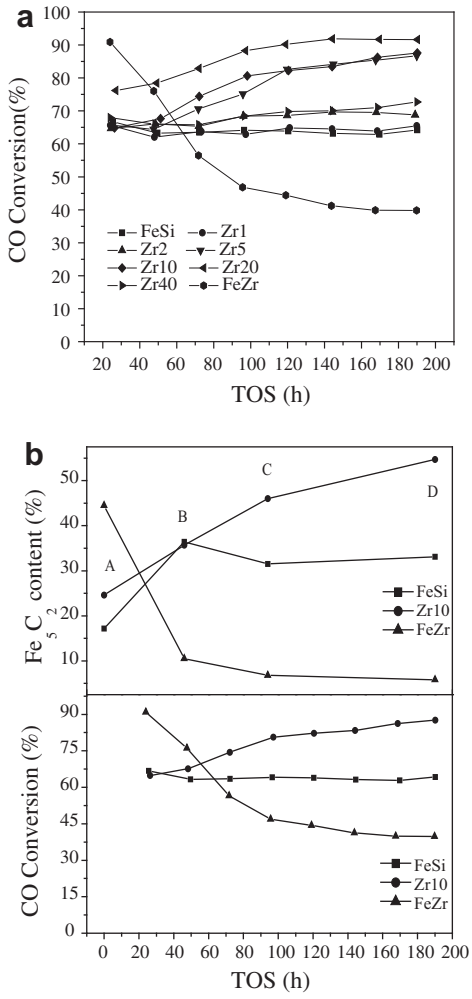

Fig. 9. (a) CO conversion as a function of time on stream of the zirconia-promoted FeSi catalysts. (b) CO conversion vs. iron carbide content of selected catalysts (A, after reduction; B, reaction for 48 h; C, reaction for 96 h; D, after reaction).

dynamic and reversible depending upon the environment in FTS reactors. Under oxidizing conditions (i.e., at high H_2O and CO_2 partial pressures), iron carbide will be oxidized to Fe_3O_4, which leads to the deactivation of iron-based FTS catalysts [52,53,58,59]. Accordingly, the Fe_3O_4 could be recarburized to iron carbides when the CO partial pressure was high [58,60]. For FeZr catalysts, high iron carbide content after activation ensured high initial activity; thus, a large amount of H_2O would be produced, which in turn oxidized the iron carbides, since the stability of iron carbide in FeZr catalysts is poor, as indicated by the H_2O oxidation experiment. Consequently, the iron carbide content decreased gradually with TOS, which deactivated the catalyst. Meanwhile, the deactivation caused by the deposition of inactive carbonaceous compounds on the catalysts' surfaces cannot be ruled out [19]. However, the χ-Fe_5C_2 content of FeSi catalysts increased slightly in the initial stage and then became stable. It is hypothesized that the two opposing processes (the oxidation of iron carbides and the recarburization of Fe_3O_4) reached a dynamic equilibrium in FeSi catalysts caused by the interaction between iron and silica. Also, the active phase could be stabilized by SiO_2 due to its strong dispersion effect, which helps to prevent sintering [61]. Therefore, the amount of iron carbide did not change significantly, and no obvious change in the CO conversion level of FeSi catalysts was observed. As concluded previously, the reduction and carburization ability of FeSi catalysts were enhanced by ZrO_2. Moreover, the stability of iron carbide was improved. It is probable that more iron carbide would be formed in Zr10 catalysts, and these species would be more stable in terms of H_2O oxidation than FeSi catalysts during FTS. As a result, the χ-Fe_5C_2 content of Zr10 catalysts increases gradually with TOS, which is in parallel with the trend of activity variation. Simultaneously, researchers found that CO dissociation was facilitated by zirconia because of the tilted CO chemisorption mode [12,62,63], which enhanced the activity of the catalysts. This promotional effect of ZrO_2 should not be ignored in the present study. For Zr40 catalysts, which contained the highest level of ZrO_2, it is postulated that more iron carbide would be oxidized because of the poor stability of iron carbide, lowering the iron carbide content in the used catalyst, and that the active sites can be covered partly by zirconia [12,14], all of which accounted for the decreased activity of Zr40 catalyst.

3.6.2. Product selectivity

The hydrocarbon product distribution of the catalysts is shown in Table 9. As can be seen, the selectivity to gaseous and light

Table 9
Activity and selectivity of the zirconia-promoted FeSi catalysts.[a,b]

Catalysts	FeSi		Zr1		Zr2		Zr5		Zr10		Zr20		Zr40		FeZr	
	72	145	72	144	72	144	72	145	72	144	72	144	72	144	72	144
TOS																
CO conversion (%)	63.5	63.2	63.7	64.5	65.4	69.7	70.6	84.2	74.4	83.4	82.9	91.9	65.8	70.0	56.5	41.2
CO + H_2 conversion (%)	51.7	51.7	52.7	53.6	54.5	58.5	57.9	67.3	59.3	65.0	62.2	69.4	54.3	57.2	46.2	35.7
Exit molar H_2/CO ratio	2.9	2.9	3.0	3.1	3.1	3.2	3.3	6.2	3.8	5.4	5.9	10.7	3.1	3.4	2.7	2.2
H_2/CO molar usage	1.4	1.4	1.4	1.4	1.4	1.4	1.5	1.4	1.4	1.4	1.3	1.4	1.5	1.5	1.4	1.6
CO_2 selectivity (mol%)	25.8	26.0	26.0	26.7	26.7	27.2	28.7	29.1	25.3	27.9	27.7	30.9	23.6	25.3	27.7	23.7
$K_p((PCO_2 \cdot PH_2)/(PCO \cdot PH_2O)$	1.6	1.6	1.7	1.8	1.9	2.1	2.1	4.4	2.0	3.4	4.1	8.9	1.5	1.8	1.9	1.2
Selectivity (wt.%)																
C_1	20.0	22.9	20.1	21.2	19.9	20.8	18.1	19.1	16.3	17.5	17.0	18.2	21.8	23.9	25.4	32.2
$C_2 - C_4$	42.5	43.3	41.9	42.1	41.0	41.9	40.2	41.9	38.5	39.4	36.2	37.0	43.3	43.4	45.9	46.4
C_5^+	37.5	33.8	38.0	36.7	39.1	37.3	41.7	39.1	45.2	43.2	46.8	44.8	34.9	32.7	28.7	21.4
C_5^+) and olefins ($C_2^= - C_4^=/C_2^0 - C_4^0$ (mol/mol)	1.1	1.0	1.1	1.1	1.2	1.1	1.4	1.2	1.5	1.3	1.4	1.2	0.9	0.8	0.4	0.3
Oxygenates[c] *(wt.%)*																
Acid	0.6	0.6	0.6	0.5	0.5	0.5	0.5	0.4	0.3	0.3	0.3	0.3	0.4	0.3	0.1	0.1
Alcohol	8.9	8.6	9.0	9.1	9.0	8.9	9.5	8.9	9.5	8.8	9.2	9.5	8.3	9.2	9.5	10.8
Others	1.2	1.1	1.3	1.3	1.2	1.2	1.9	1.8	1.1	1.1	0.9	0.8	1.4	1.4	1.0	0.9

[a] Reaction condition: 270 °C, 1.5 MPa, $H_2/CO = 2.0$, and GHSV = 2000 h^{-1}.
[b] Max error = ±3%.
[c] Oxygenates in total CH and oxygenates.

hydrocarbons (methane and C_2–C_4) was suppressed, whereas that to heavy hydrocarbons (C_5^+) and olefins ($C_2^= - C_4^=/C_2^o - C_4^o$) was enhanced by the incorporation of ZrO_2. Bukur et al. [61] found that catalysts with high iron carbide content showed excellent selectivity to C_5^+ hydrocarbons and a high olefin/paraffin ratio. The reasons for this type of behavior were not clearly understood but may be related to the fact that high iron carbide content enhanced the chain propagation reaction and suppressed the hydrogenation ability of catalysts. This is consistent with the latest results reported by Yu et al. [64]. In the present study, the trend of hydrocarbon selectivity variation correlated well with the iron carbide content of the catalysts; i.e., the higher the χ-Fe_5C_2 content, the better the selectivity to C_5^+ hydrocarbons.

Table 9 indicated that the acid content decreased with increasing ZrO_2 loading, whereas the alcohol content increased, which can be ascribed to the promotional effect of ZrO_2, since FeZr catalyst showed the highest alcohol content but the lowest acid content among all the catalysts. Actually, it is reported that alcohols could be formed on ZrO_2 via CO hydrogenation and that ZrO_2 was an effective support for alcohols synthesis catalysts [65]. However, this behavior of ZrO_2 is expected to be well understood by investigations into the detailed mechanisms for the formation of oxygenates.

4. Conclusions

In this study, multiple methods (FTIR, XPS, TPR, XRD, TEM, and MES) were applied to investigate the influence of zirconia on iron–silica interaction, and its effects on the physicochemical properties and FTS performance of the ZrO_2-modified FeSi catalysts were examined as well.

No obvious change was observed in the textural properties of the catalysts with the addition of ZrO_2 since the dispersion state of iron oxides is governed by the strong dispersion effect of SiO_2. An Fe–O–Si-like bond was observed in SiO_2-containing catalysts due to the strong iron–silica interaction, which changed the binding energy of Fe2*p*, Si2*p*, and O1*s* due to partial electron transfer from Fe–O_{Fe} units to Si species. This bond could also be weakened by the addition of ZrO_2, presumably by forming Zr–O–Si linkages. As a result, both the reduction and carburization degree were enhanced. Interestingly, the stability of iron carbides was also improved.

During the FTS reaction, more iron carbides formed in the FeSi catalyst promoted with a proper amount of zirconia (with a loading range from Zr2 to Zr20). Moreover, these species exhibit better stability under H_2O-containing atmospheres. Consequently, the iron carbide content increased gradually with TOS, which increased the activity and shifted the products to heavier hydrocarbons. The selectivity to acids decreased, but the alcohol content increased with increasing zirconia loading. These results are indicative of a complex metal–silica interaction and promotional effect of zirconia that require further investigation.

Acknowledgments

We thank the National Outstanding Young Scientists Foundation of China (20625620) and the 973 Project from the Ministry of Science and Technology of China (Grant 2011CB201401). This work is also supported by Synfuels CHINA Co., Ltd.

Appendix A. Supplementary material

Supplementary data associated with this article can be found, in the online version, at doi:10.1016/j.jcat.2011.01.005.

References

[1] D.B. Bukur, C. Sivaraj, Appl. Catal. A Gen. 231 (2002) 201.
[2] C.H. Zhang, H.J. Wan, Y. Yang, H.W. Xiang, Y.W. Li, Catal. Commun. 7 (2006) 733.
[3] Y. Yang, H.W. Xiang, L. Tian, H. Wang, C.H. Zhang, Z.C. Tao, Y.Y. Xu, B. Zhong, Y.W. Li, Appl. Catal. A Gen. 284 (2005) 105.
[4] R. Zhao, J.G. Goodwin, K. Jothimurugesan, S.K. Gangwal, J.J. Spivey, Ind. Eng. Chem. Res. 40 (2001) 1320.
[5] H.J. Wan, B.S. Wu, Z.C. Tao, T.Z. Li, X. An, H.W. Xiang, Y.W. Li, J. Mol. Catal. A Chem. 260 (2006) 255.
[6] D.B. Bukur, X. Lang, D. Mukesh, W.H. Zimmerman, M.P. Rosynek, C.P. Li, Ind. Eng. Chem. Res. 29 (1990) 1588.
[7] E. de Smit, F.M.F. de Groot, R. Blume, M. Havecker, A. Knop-Gericke, B.M. Weckhuysen, Phys. Chem. Chem. Phys. 12 (2010) 667.
[8] D.B. Bukur, D. Mukesh, S.A. Patel, Ind. Eng. Chem. Res. 29 (1990) 194.
[9] Y. Yang, H.W. Xiang, Y.Y. Xu, L. Bai, Y.W. Li, Appl. Catal. A Gen. 266 (2004) 181.
[10] Y.Q. Zhang, H.W. Xiang, B. Zhong, Q. Wang, Pet. Sci. Technol. 17 (1999) 981.
[11] G.R. Moradi, M.M. Basir, A. Taeb, A. Kiennemann, Catal. Commun. 4 (2003) 27.
[12] S. Ali, B. Chen, J.G. Goodwin, J. Catal. 157 (1995) 35.
[13] B. Jongsomjit, S. Kittiruangrayub, P. Praserthdam, Mater. Chem. Phys. 105 (2007) 14.
[14] J. Hong, W. Chu, P.A. Chernavskii, A.Y. Khodakov, Appl. Catal. A Gen. 382 (2010) 28.
[15] C.H. Zhang, Y. Yang, B.T. Teng, T.Z. Li, H.Y. Zheng, H.W. Xiang, Y.W. Li, J. Catal. 237 (2006) 405.
[16] C.R.F. Lund, J.A. Dumesic, J. Catal. 72 (1981) 21.
[17] S. Yuen, J.E. Kubsh, J.A. Dumesic, N. Topsoee, H. Topsoee, Y. Chen, J. Phys. Chem. 86 (2002) 3022.
[18] S. Bruni, F. Cariati, M. Casu, A. Lai, A. Musinu, G. Piccaluga, S. Solinas, Nanostruct. Mater. 11 (1999) 573.
[19] E.d. Smit, B.M. Weckhuysen, Chem. Soc. Rev. 37 (2008) 2758.
[20] J.M. Zhao, Z. Feng, F.E. Huggins, G.P. Huffman, Energy Fuels 8 (1994) 38.
[21] J. Zhao, F.E. Huggins, Z. Feng, F.L. Lu, N. Shah, G.P. Huffman, J. Catal. 143 (1993) 499.
[22] R. Szostak, V. Nair, T.L. Thomas, J. Chem. Soc. Faraday Trans. 83 (1987) 487.
[23] S. Bordiga, R. Buzzoni, F. Geobaldo, C. Lamberti, E. Giamello, A. Zecchina, G. Leofanti, G. Petrini, G. Tozzola, G. Vlaic, J. Catal. 158 (1996) 486.
[24] D. Scarano, A. Zecchina, S. Bordiga, F. Geobaldo, G. Spoto, J. Chem. Soc. Faraday Trans. 89 (1993) 4123.
[25] U. Schwertmann, H. Thalmann, Clay Miner. 11 (1976) 189.
[26] J.E. Iglesias, M. Ocana, C.J. Serna, Appl. Spectrosc. 44 (1990) 418.
[27] M. Gotic, S. Music, J. Mol. Struct. 834–836 (2007) 445.
[28] F.R. van den Berg, M.W.J. Crajé, A.M. van der Kraan, J.W. Geus, Appl. Catal. A Gen. 242 (2003) 403.
[29] F.R. van den Berg, M.W.J. Crajé, P.J. Kooyman, A.M. van der Kraan, J.W. Geus, Appl. Catal. A Gen. 235 (2002) 217.
[30] J.B. Butt, Catal. Lett. 7 (1991) 61.
[31] H.J.M. Bosman, A.P. Pijpers, A.W.M.A. Jaspers, J. Catal. 161 (1996) 551.
[32] X.W. Du, X.B. Yuan, Analysis Techniques in Materials Science, TianJin University Press, TianJin, 2006. p. 135.
[33] K.Y. Li, D.F. Xue, J. Phys. Chem. A 110 (2006) 11332.
[34] Y.G. Zhang, Inorg. Chem. 21 (1982) 3886.
[35] G. Mountjoy, R. Anderson, R.J. Newport, M.E. Smith, J. Phys. Condens. Matter 12 (2000) 3505.
[36] J.M. Kim, S.M. Chang, S. Kim, K.-S. Kim, J. Kim, W.-S. Kim, Ceram. Int. 35 (2009) 1243.
[37] Z.G. Wu, Y.X. Zhao, D.S. Liu, Micropor. Mesopor. Mater. 68 (2004) 127.
[38] S.W. LEE, R.A.C. Sr, J. Mater. Sci. 23 (1988) 2951.
[39] F.d. Monte, W. Larsen, J.D. Mackenzie, J. Am. Ceram. Soc. 83 (2000) 1506.
[40] H.J. Wan, B.S. Wu, C.H. Zhang, H.W. Xiang, Y.W. Li, B.F. Xu, F. Yi, Catal. Commun. 8 (2007) 1538.
[41] A.F.H. Wielers, A.J.H.M. Kock, C.E.C.A. Hop, J.W. Geus, A.M. van Der Kraan, J. Catal. 117 (1989) 1.
[42] N. Lohitharn, J.G. Goodwin Jr, E. Lotero, J. Catal. 255 (2008) 104.
[43] R. Zboril, M. Mashlan, D. Petridis, Chem. Mater. 14 (2002) 969.
[44] Y. Okamoto, T. Kubota, Y. Ohto, S. Nasu, J. Phys. Chem. B 104 (2000) 8462.
[45] W. Kundig, H. Bommel, G. Constaba, Rh. Lindqui, Phys. Rev. 142 (1966) 327.
[46] Am. Vanderkr, Phys. Status Solidi A 18 (1973) 215.
[47] B. Kolk, A. Albers, I.R. Leith, M.G. Howden, Appl. Catal. 37 (1988) 57.
[48] H. Dlamini, T. Motjope, G. Joorst, G.t. Stege, M. Mdleleni1, Catal. Lett. 78 (2002) 201.
[49] M. Boudart, A. Delbouille, J.A. Dumesic, S. Khammouma, H. Topsøe, J. Catal. 37 (1975) 486.
[50] E.S. Lox, G.B. Marin, E. De Grave, P. Bussière, Appl. Catal. 40 (1988) 197.
[51] N. Sirimanothan, H.H. Hamdeh, Y.Q. Zhang, B.H. Davis, Catal. Lett. 82 (2002) 181.
[52] M.E. DRY, Catal. Lett. 7 (1990) 241.
[53] W.S. Ning, N. Koizumi, H. Chang, T. Mochizuki, T. Itoh, M. Yamada, Appl. Catal. A Gen. 312 (2006) 35.
[54] A. Feller, M. Claeys, E.v. Steen, J. Catal. 185 (1999) 120.
[55] G.B. Raupp, W.N. Delgass, J. Catal. 58 (1979) 348.
[56] J.B. Butt, Catal. Lett. 7 (1991) 83.

[57] C.N. Satterfield, R.T. Hanlon, S.E. Tung, Z.M. Zou, G.C. Papaefthymiou, Ind. Eng. Chem. Prod. Res. Dev. 25 (1988) 401.
[58] A. Sarkar, D. Seth, A.K. Dozier, J.K. Neathery, H.H. Hamdeh, B.H. Davis, Catal. Lett. 117 (2007) 1.
[59] S. Li, R.J. O'Brien, G.D. Meitzner, H. Hamdeh, B.H. Davis, E. Iglesia, Appl. Catal. A Gen. 219 (2001) 215.
[60] S. Li, W. Ding, G.D. Meitzner, E. Iglesia, J. Phys. Chem. B 106 (2002) 85.
[61] D.B. Bukur, L. Nowicki, R.K. Manne, X.S. Lang, J. Catal. 155 (1995) 366.
[62] H.P. Withers, K.F. Eliezer, J.W. Mitchell, Ind. Eng. Chem. Res. 29 (1990) 1807.
[63] M. Ichikawa, T. Fukushima, J. Phys. Chem. 89 (1985) 1564.
[64] G.B. Yu, B. Sun, Y. Pei, S.H. Xie, S.R. Yan, M.H. Qiao, K.N. Fan, X.X. Zhang, B.N. Zong, J. Am. Chem. Soc. 132 (2010) 935.
[65] Y.H. Sun, P.A. Sermon, J. Chem. Soc. Chem. Commun. 16 (1993) 1242.